Sargassum Polycystum–Mediated Ag@ZrO_2 Nanocomposite for Sulfinpyrazone Detection and Antimicrobial Activity

M. Padmaja[1,2#], Dr.M.E. Rani[2*]

[1]*Department of Chemistry, MRR GOVT. Arts & Science Degree College, Udayagiri, SPSR Nellore Dist., - 524226, Andhra Pradesh, India.*

[2#]*Research Scholar,*[2*] *Professor, Department of Chemistry, Rayalaseema University, Kurnool-518007, Andhra Pradesh, India,*

***Abstract*—The bio-synthesis of nanoparticles from natural sources is highly desirable due to its minimal environmental impact. This study focuses on the biogenic synthesis of Ag@ZrO_2 nanoparticles using an aqueous extract of *sargassum polycystum (brown algae)* seaweeds, an invasive seaweed species that disrupts aquatic ecosystems by covering water surfaces. The biosynthesised Ag@ZrO_2 nanocomposite development of an electrochemical sensor for real-time sulfinpyrazone drug monitoring in serum samples. The electrochemical sensor was fabricated using an Ag@ZrO_2 nanocomposite-modified glassy carbon electrode (Ag@ZrO_2/GCE). The synthesized nanoparticles were characterized using UV–Visible Spectroscopy, Fourier Transform Infrared Spectroscopy, X-Ray Diffraction, and Scanning Electron Microscopy. Electrochemical analysis demonstrated a linear correlation between the differential pulse voltammetry peak current and sulfinpyrazone concentrations ranging from 0.05 to 100.0 µM, with a detection limit of 0.028 µM. Long-term stability assessments revealed that the sensor retained 97.55% of its initial response after 30 days, indicating excellent stability and repeatability. Furthermore, the synthesized nanoparticles demonstrated pronounced antibacterial efficacy against Bacillus subtilis and Escherichia coli, underscoring their potential pharmacological and therapeutic applications. These findings suggest that Ag@ZrO_2 nanoparticles have significant potential for biomedical and pharmaceutical applications, while the developed electrochemical sensor offers a reliable platform for sulfinpyrazone detection in clinical diagnostics.**

***Index Terms*—sargassum polycystum; sulfinpyrazone; nanoparticles; antibacterial.**

I. INTRODUCTION

As the demand for waste reduction and sustainable development continues to rise, implementing the core principles of green chemistry has become increasingly important [1]. This has led to a growing need for eco-friendly alternatives in nanoparticle synthesis [2]. The adoption of green methodologies across various technological fields is expanding rapidly, driven by concerns over the environmental and health hazards associated with conventional chemical and physical processes [3]. Nanotechnology, known for its cutting-edge innovations and extensive applications in numerous scientific and technological domains, including biomedical sciences, has gained significant interest [4]. Traditional methods for nanoparticle production primarily rely on chemical and physical techniques, which are often costly and pose risks to both the environment and human health [5]. In contrast, biosynthesis presents a sustainable, environmentally friendly, cost-effective, high-yielding, and energy-efficient approach to nanoparticle synthesis [6]. Researchers are now focusing on biosynthesis using biological entities such as plants, bacteria, fungi, and enzymes. Among these, algaes are particularly noteworthy as natural nano-factories, capable of producing various nanoparticles, through both living and dried biomass [7, 8].

Zirconia has garnered significant interest among researchers due to its diverse applications in oxygen sensors, fuel cells, transparent optical devices, catalysis, and fire-retardant materials in material science [9]. Zirconium oxide (ZrO_2), recognized for its superior electrical, thermal, optical, and mechanical characteristics, is considered one of the most essential ceramic materials, enabling its use across a wide array of applications [10]. With a broad band gap ranging from 5.0 to 7.0 eV, depending on the synthesis method, zirconia is widely utilized in manufacturing gas sensors, metal oxide semiconductors, ceramic devices, fuel cell electrolytes, catalysts, catalyst support materials, and thermal barrier coatings [11,12]. In recent years, zirconia has attracted significant attention in biomedical applications [13]. Additionally, there has been a growing interest in zirconia nanoparticles as antimicrobial agents due to their biocompatibility and non-cytotoxic nature [14]. The antimicrobial efficacy of nanoparticles is influenced by factors such as size, stability, and concentration in the growth medium. Other characteristics, including morphology, surface charge, and surface coating, also play a crucial role in determining their antibacterial activity [15]. ZrO_2 has found widespread application in electrochemical sensors [16]. Notably, nanostructured ZrO_2 particles exhibit large specific surface areas, which play a crucial role in improving toxin detection capabilities. Additionally, the material's high chemical stability and non-toxic nature make it a preferred choice for such applications. Studies indicate that integrating Ag with ZrO_2 nanoparticles can further enhance sensor performance [17].

Various analytical techniques have been explored for the quantification of sulfinpyrazone, each offering distinct advantages and limitations. Among these, high-performance liquid chromatography (HPLC) [18], liquid chromatography-mass spectrometry (LC-MS) [19], and a range of spectroscopic methods are commonly utilized. However, these approaches often come with challenges such as complex sample preparation, high costs, operational intricacies, and limitations in sensitivity and selectivity [20]. Electrochemical techniques have emerged as a promising alternative, particularly for real-time and on-site applications in pharmaceutical and clinical settings [21, 22]. Their key advantages include high sensitivity, rapid analysis, and the potential for miniaturization. The incorporation of nanostructures into electrochemical sensors has further enhanced the electrocatalytic properties of electrodes, leading to improved sensitivity and selectivity in sulfinpyrazone detection [23]. Compared to other sensor types, electrochemical sensors offer several benefits. Their high sensitivity enables the detection of even the slightest variations in the chemical environment, making them highly effective for monitoring drug concentrations [24]. Additionally, their ability to provide real-time data is crucial in dynamic pharmaceutical applications. Furthermore, electrochemical sensors are generally compact and cost-effective, facilitating their widespread use across diverse fields [25]. The integration of electrochemical methods with nanostructures holds great promise for advancing sensor technology [26]. This combination lays the groundwork for precise, reliable, and efficient analysis of sulfinpyrazone, ultimately contributing to the development of enhanced detection systems for this essential chemotherapeutic drug [27].

This research investigates the eco-friendly synthesis and detailed characterization of ZrO_2 and Ag@ZrO_2 nanoparticles using *sargassum polycystum* seaweed extract. The synthesized nanocomposites were thoroughly analyzed through UV–Visible Spectroscopy (UV-Vis.), Fourier Transform Infrared Spectroscopy (FTIR), X-Ray Diffraction (XRD), Scanning Electron Microscopy (SEM) and Energy-Dispersive X-ray spectroscopy (EDX) to determine their structural, morphological, and elemental properties. The synthesized Ag@ZrO_2 nanocomposites displayed remarkable antibacterial, and electrochemical sensing capabilities, showing exceptional efficiency in detecting sulfinpyrazone in real serum samples. Furthermore, these nanoparticles offer significant advantages, including cost-effectiveness, environmental sustainability, stability, and biocompatibility, highlighting their potential for a wide range of biomedical and environmental applications.

II. EXPERIMENTAL

A. Materials and methods

Silver nitrate ($AgNO_3$, 99.99%), zirconyl tetrachloride octahydrate ($ZrCl_4 \cdot 8H_2O$, 98%), Potassium permanganate ($KMnO_4$), potassium tetrachloropalladate, and various other metal salts were obtained from Sigma-Aldrich. The 0.1 M phosphate buffer solution stock solutions were prepared by adding of required amounts of dihydrogen phosphate (0.1M) and disodium phosphate (0.1M). A sulfinpyrazone stock solution was prepared by dissolving 1000 mg of sulfinpyrazone in ultra-pure water and diluting it to a final volume of 1000 mL. Working solutions were then prepared by diluting the stock solution as needed. All chemicals used were of analytical grade and were utilized without further purification. Double-distilled water was employed for preparing all aqueous stock solutions.

B. Characterization

The synthesized Ag@ZrO_2 nanoparticles derived from *Sargassum polycystum* seaweed extract were verified and characterized using a double-beam UV–visible spectrophotometer (Shimadzu PC 1650) within the 200–800 nm range to detect the characteristic peak indicative of Ag@ZrO_2 nanoparticle formation. Fourier transform infrared spectroscopy (Bruker Alpha-P infrared spectrophotometer, Thermo-Scientific, Austin, TX, USA) was employed to identify functional groups and phytoconstituents responsible for the reduction and stabilization of the nanoparticles. Additionally, a scanning electron microscope, coupled with energy dispersive X-ray analysis (EDX) (JEOL, JSM IT 200, Japan), and an X-ray diffractometer (Bruker D8 ADVANCE X-ray powder diffractometer) were utilized to examine surface morphology, elemental composition, particle size, and shape of the green-synthesized Ag@ZrO_2 nanoparticles.

C. Harvesting and Processing of Seaweed Extracts

The *sargassum polycystum (brown algae)* seaweed was collected from the coastal region of Tamil Nadu in the Bay of Bengal. After collection, the sample was immediately transported to the laboratory and thoroughly cleaned with tap and distilled water to remove epiphytes and debris. For taxonomic identification, a portion of the sample was preserved in 5% formalin. The remaining seaweed was air-dried in the shade at 35 ± 2 °C. Once dried, the samples were finely ground into a powder and stored in tightly sealed containers for further research, following standard literature protocols.

Using a magnetic stirrer, 10 g of seaweed powder was mixed with 100 mL of distilled water in a flask and heated to 70 °C for 30 minutes in a water bath. The mixture was then continuously shaken overnight using a shaker. After thorough filtration through filter paper, the extract was cooled and stored for the biosynthesis process. The resulting filtrate was used as a bio-reducing agent for the synthesis of ZrO_2 and Ag@ZrO_2 nanoparticles.

D. Biosynthesis of ZrO_2 and Ag@ZrO_2 Nanoparticles

A 100 mL flask was filled with 10 mL of algae extract, followed by the addition of 25 mL of a 20 mM zirconium oxychloride precursor ($ZrOCl_4$). The pH of the reaction mixture was then adjusted to above ~10 by gradually adding 1.0×10^3 mM NaOH dropwise while stirring continuously for two hours at 60 °C. The formation of ZrO_2 nanoparticles was indicated by the appearance of a cloudy white colour. To eliminate any unreacted solutes and phytochemicals, the reaction product was centrifuged at 3000 rpm for 15 minutes. The resulting brown precipitate was washed five times with deionized water and then dried in an oven at 60 °C for 48 hours. Similarly, 20 mL of algae extract was mixed with 25 mL of 20 mM zirconium oxychloride precursor ($ZrOCl_4$) and 10 mL of 5.0 mM silver nitrate ($AgNO_3$) in a 100 mL flask. The pH was raised above 10 by adding 1 M NaOH dropwise, followed by stirring at 60 °C for two hours. The brown colour precipitate indicated Ag@ZrO_2 nanoparticle formation. The product was centrifuged at 3000 rpm for 15 minutes, washed five times with deionized water, and dried at 60 °C for 48 hours.

E. Electrochemical study

A three-electrode cell setup equipped with an Autolab PGSTAT 30 was used to assess the electrocatalytic performance of biosynthesised ZrO_2 and Ag@ZrO_2 nanocomposites. A platinum wire served as the counter electrode, while a saturated Ag/AgCl electrode functioned as the reference electrode. The working electrode comprised a glassy carbon electrode coated with the nano-catalysts (ZrO_2 and Ag@ZrO_2). The preparation of the working electrode involved polishing a glassy carbon electrode with 0.05 mm aluminium oxide paste on a chamois cloth, followed by rinsing in acetone, ethanol, and ultra-pure water under ultrasonication for 10 min. Subsequently, 10 mg of electro-catalysts (ZrO_2 and Ag@ZrO_2) dispersed in a nafion to obtain a uniformly dispersed suspension for alternation of the GCE surface. In order to prepare the catalyst suspension, 20 µL were carefully deposited onto the surface of the working electrode and allowed to dry at room temperature and to remove any non-bound nanoparticles from the surface, the electrode was washed through phosphate buffer solution. The electrode was then dried and ready for use. Before an electrochemical assessment, the electrolyte solution underwent degassing with nitrogen gas for approximately 5 min to eliminate dissolved oxygen.

F. Antimicrobial activity

The antimicrobial efficacy of green-synthesized zirconium oxide (ZrO_2), silver–zirconium oxide nanocomposite (Ag@ZrO_2), Sargassum polycystum extract, and the standard antibiotic gentamycin was evaluated against two pathogenic bacterial strains: the Gram-positive Bacillus subtilis and the Gram-negative Escherichia coli. The assessment was performed using the agar well diffusion technique [28, 29]. Each sample was appropriately dissolved in physiological saline solution (0.9% NaCl), which served as the solvent control and exhibited no inhibitory effect on any of the tested microbial strains. Gentamycin was employed as the positive control to validate the antimicrobial performance of the synthesized materials.

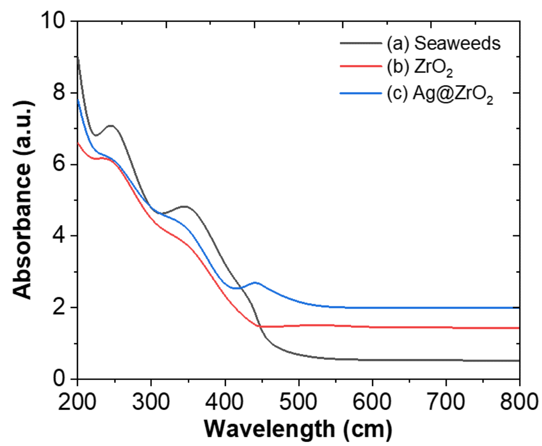

Fig. 1. UV-Visible spectra of *sargassum polycystum* extract (a); ZrO_2 (b); Ag@ZrO_2 (c).

III. RESULTS AND DISCUSSION

A UV–Visible spectrophotometer was employed to examine the optical absorption behavior of the bio-synthesized nanoparticles. Figure 1, illustrates the UV–Vis absorption spectra of *Sargassum polycystum* seaweed extract, ZrO_2, and Ag@ZrO_2 nanoparticles. The *Sargassum polycystum* extract exhibited pronounced absorption bands in the ultraviolet region, with peaks observed at 265 nm and 354 nm (Fig. 1a). The ZrO_2 nanoparticles displayed a broad absorption profile within the UV region, showing peaks at approximately 240 nm and 340 nm, which can be ascribed to electrostatic interactions between Zr^{2+} ions and phytochemical constituents present in the seaweed extract (Fig. 1b). Furthermore, an additional absorption band appearing at around 440 nm in the visible region corresponds to the surface plasmon resonance (SPR) of silver nanoparticles, confirming the successful formation of Ag species (Fig. 1c). The enhanced intensity of the SPR band relative to the ZrO_2 spectrum indicates that the incorporation of Ag notably alters the optical and electronic characteristics of the nanocomposite.

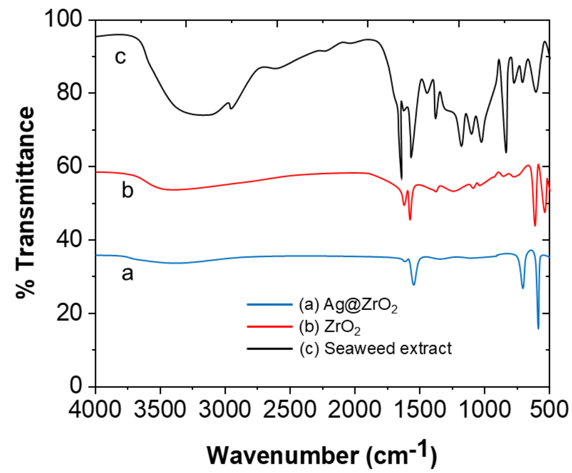

Fig. 2. FTIR spectra of (c) Sargassum polycystum seaweed extract, (b) ZrO_2, and (a) Ag@ZrO_2 nanocomposites.

The functional groups associated with the synthesized nanoparticles were characterized through Fourier Transform Infrared (FTIR) spectroscopy. Figure 2, presents the FTIR spectra of *Sargassum polycystum* seaweed extract (Fig. 2c), ZrO_2 nanoparticles (Fig. 2b), and Ag@ZrO_2 nanocomposites (Fig. 2a). The *Sargassum polycystum* extract exhibited a broad absorption band at 3450.40 cm^{-1}, corresponding to the O–H stretching vibration of hydroxyl groups, along with a minor C–H stretching vibration near 2930.14 cm^{-1}. A prominent band appearing around 534.45 cm^{-1} in the ZrO_2 spectrum confirms the formation of the Zr–O bond, characteristic of the ZrO_2 nanostructure. Moreover, the observed peaks at approximately 3460.35 cm^{-1} and 3360.45 cm^{-1} are attributed to hydroxyl stretching vibrations associated with phenolic and alcoholic constituents in the seaweed extract. The absorption band near 2920.45 cm^{-1} is assigned to C–H stretching, while those around 1640.50 cm^{-1} and

1540.30 cm^{-1} correspond to H–O–H bending vibrations (Fig. 2a). A similar bending mode near 1650.20 cm^{-1} was also identified in the seaweed extract spectrum. These spectral signatures collectively confirm the presence of bioactive phytochemicals act as natural reducing and stabilizing agents in the synthesis of Ag@ZrO_2 nanoparticles.

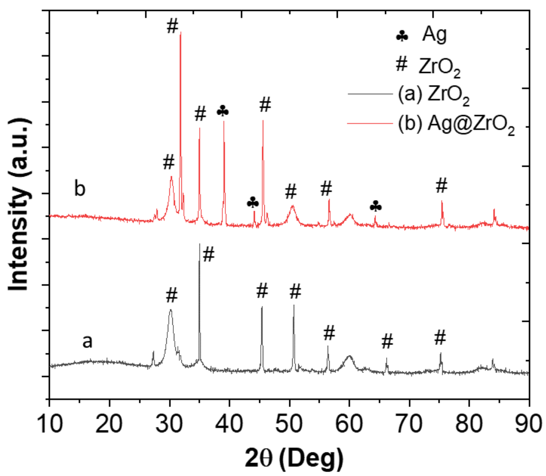

Fig. 3. X-ray diffraction (XRD) patterns of (a) ZrO_2 and (b) Ag@ZrO_2 spinel nanocomposites.

The crystalline structure of the Ag@ZrO_2 nanocomposite was characterized using X-ray diffraction (XRD) analysis, as shown in Fig. 3. The observed diffraction peaks at 2θ values of 30.46°, 35.43°, 45.50°, 56.26°, 60.17°, 66.94°, 75.02°, and 85.04° correspond to the (101), (110), (112), (103), (211), (202), (220), (213), and (310) lattice planes of monoclinic ZrO_2 (Fig. 3a) which closely match the reference data from JCPDS card No. 89-7710 [30]. The absence of any additional or impurity peaks confirms the high crystallinity and phase purity of the synthesized nanocomposite. Moreover, distinct peaks at 2θ values of 38.9°, 44.8°, and 64.5° are indexed to the (111), (200), and (220) planes (Fig. 3b) of face-centered cubic (fcc) silver, consistent with JCPDS card No. 87-0720 [31]. These diffraction features confirm the successful incorporation of metallic Ag within the ZrO_2 matrix without the emergence of secondary or unwanted phases. The mean crystallite size, estimated using Scherrer's equation, was found to be approximately ~21 nm, indicating the nanoscale nature of the synthesized Ag@ZrO_2 material [32].

Scanning Electron Microscopy (SEM) was employed to investigate the morphological and surface characteristics of the synthesized ZrO_2 and Ag@ZrO_2 nanoparticles. Figures 4(a) and 4(b) depict the FE-SEM micrographs of ZrO_2 and Ag@ZrO_2 nanoparticles at a magnification of 500 nm, revealing a well-defined nanostructured morphology with uniformly distributed particles. The particle sizes were found to be relatively consistent, ranging between 25 and 35 nm. The nanocomposite samples exhibited irregularly aggregated nanograins, indicative of slight agglomeration, as shown in Fig. 4.

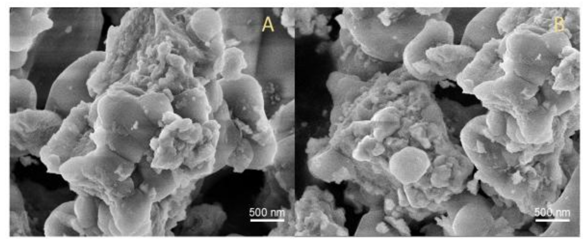

Fig. 4. FE-SEM micrographs of (A) ZrO_2 and (B) Ag@ZrO_2 spinel nanocomposites.

The elemental composition of the synthesized materials was further examined using Energy Dispersive X-ray (EDX) spectroscopy, as illustrated in Fig. 5. The EDX spectra display prominent peaks corresponding to zirconium (Zr), silver (Ag), and oxygen (O), confirming the presence of these elements in the synthesized nanocomposites. The experimentally obtained elemental ratios were in close agreement with the theoretically expected stoichiometric values, demonstrating good compositional uniformity throughout the sample. Distinct peaks in the 0–4.0 keV energy range correspond to the crystalline Ag@ZrO_2 nanocomposite, validating its successful formation [33].

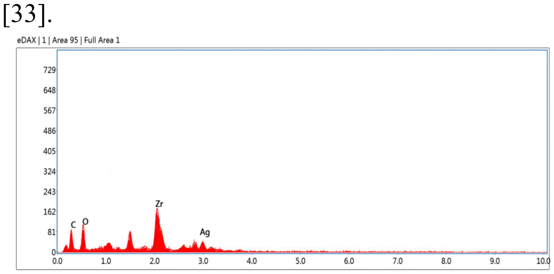

Fig. 5. Energy-dispersive X-ray (EDX) spectrum of Ag@ZrO_2 nanocomposites.

Electroanalysis of sulfinpyrazone

Figure 6 illustrates the cyclic voltammograms (CVs) of various electrodes like bare glassy carbon electrode (GCE), ZrO_2-modified GCE, and Ag@ZrO_2-modified GCE, recorded in phosphate buffer solution (0.1M; pH 6.0) at a scan rate of 20 mV/s in the absence of sulfinpyrazone. As shown in Figures 6a–6c, no distinct redox/oxidation peaks were observed under these conditions. However, upon the addition of sulfinpyrazone, the cyclic voltammograms of the bare GCE (Fig. 7c), ZrO_2/GCE (Fig. 7b), and Ag@ZrO_2/GCE (Fig. 7a) exhibited prominent anodic and cathodic peaks, confirming the electrochemical activity of the analyte at the modified electrodes. The enhanced response of the Ag@ZrO_2/GCE electrode can be attributed to strong interactions between sulfinpyrazone molecules and the nanocomposite-modified surface, which facilitated improved adsorption [34]. The electrochemical behavior of sulfinpyrazone in phosphate buffer (pH 6.0) follows a quasi-reversible mechanism. The oxidation peaks appeared at −0.89 V for ZrO_2/GCE, and 0.86 V for Ag@ZrO_2/GCE and there is no significant response to bare GC electrode, indicating that the Ag@ZrO_2-modified electrode exhibited a more intense oxidation response relative to the unmodified and ZrO_2-modified counterparts. This enhancement arises from the high surface area and superior electron transfer capability of Ag@ZrO_2, which promotes efficient analyte adsorption and facilitates rapid electrochemical reactions [35]. Further analysis revealed that sulfinpyrazone undergoes an irreversible, diffusion-controlled anodic oxidation process in phosphate buffer (pH 6.0) at the Ag@ZrO_2/GCE surface, involving the transfer of two electrons and two protons to form the corresponding oxidation product. Based on experimental observations and supporting literature, a plausible oxidation mechanism for sulfinpyrazone at the Ag@ZrO_2/GCE interface has been proposed (Fig. 8). In this mechanism, the Ag@ZrO_2 nanocomposite serves as a conductive matrix, enhancing electron transport efficiency. The synergistic interaction between ZrO_2 and Ag nanoparticles contributes to improved catalytic activity, stability, and sensitivity, thereby optimizing sulfinpyrazone oxidation [36].

To further evaluate the sensing performance, differential pulse voltammetry (DPV) was conducted using bare GCE, ZrO_2/GCE, and Ag@ZrO_2/GCE electrodes. As illustrated in Fig. 9c, the bare glassy carbon electrode (GCE) exhibited no significant electrochemical response, indicating sluggish electron transfer kinetics at its unmodified surface. In contrast, the ZrO_2-modified electrode (Fig. 9b) displayed a significantly enhanced current response, likely due to the catalytic role of the bio-synthesized ZrO_2 in facilitating sulfinpyrazone oxidation. The Ag@ZrO_2/GCE electrode (Fig. 9a) demonstrated the highest electrochemical signal intensity, attributed to the synergistic catalytic behavior of Ag and ZrO_2 and the superior electrical conductivity of the Ag@ZrO_2 nanocomposite, which accelerates electron transfer during oxidation [37]. Consequently, the optimized Ag@ZrO_2/GCE electrode exhibited well-defined, high-intensity peaks, establishing its suitability for precise and sensitive electrochemical detection of sulfinpyrazone.

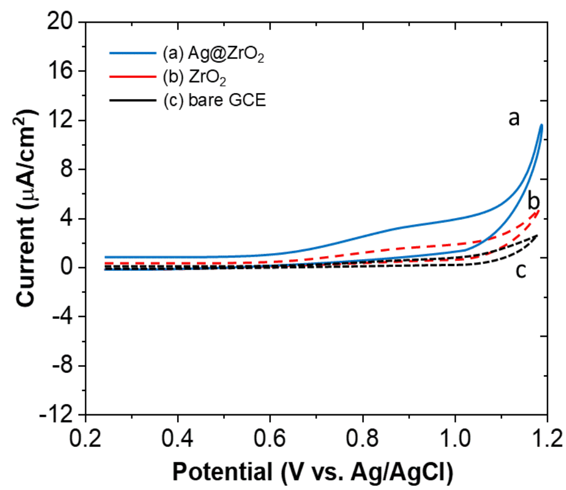

Fig. 6. Cyclic voltammetric (CV) responses of (c) bare GCE, (b) ZrO_2/GCE, and (a) Ag@ZrO_2/GCE electrodes recorded within a potential window of 0.2–1.2 V at a scan rate of 25 mV s^{-1} in 0.1 M phosphate buffer solution (pH 6.0).

The electrochemical behavior of sulfinpyrazone was examined in different supporting electrolytes, including Britton–Robinson, sodium acetate–acetic acid, and phosphate buffers. Among these, phosphate buffer exhibited the most stable and well-defined electrochemical response. The effect of pH (2.0–10.0) on the anodic peak current was studied using 0.1 M phosphate buffer, with the maximum peak observed at pH 6.0, which was selected as the optimal medium (Fig. 10). The current increased from pH 2.0 to 6.0 and decreased thereafter, likely due to electrostatic repulsion between negatively charged sulfinpyrazone and the nanocomposite surface at higher pH levels. The oxidation peak potential (E_p) varied linearly with pH, with a slope of 0.0589 V/pH, consistent with the Nernstian value, indicating that the redox process involves an equal number of electrons and protons approximately two protons, or one per electron, in the electro-oxidation of sulfinpyrazone [36].

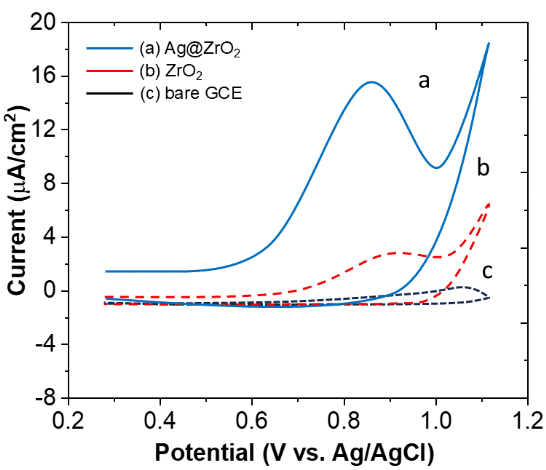

Fig. 7. Cyclic voltammetric (CV) responses of (c) bare GCE, (b) ZrO_2/GCE, and (a) Ag@ZrO_2/GCE electrodes recorded over a potential range of 0.2–1.2 V at a scan rate of 25 mV s^{-1} in 0.1 M phosphate buffer (pH 6.0) containing 6.0 μM sulfinpyrazone.

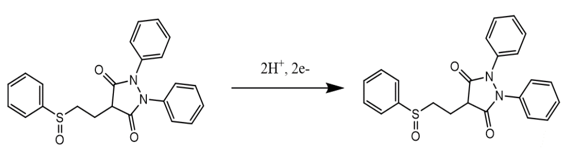

Fig. 8. Proposed electrochemical mechanism of drug of 1,2-diphenyl-4-(2-(phenylsulfinyl) ethyl) pyrazolidine-3,5-dione (sulfinpyrazone) on modified Ag@ZrO_2/GCE.

Voltammetric performance of the fabricated sensor

Key electroanalytical parameters, such as the detection limit, linear dynamic range, reproducibility, and repeatability, were evaluated to determine the analytical performance and practical applicability of the Ag@ZrO_2-modified glassy carbon electrode (Ag@ZrO_2/GCE) for sulfinpyrazone detection. The differential pulse voltammograms recorded at the Ag@ZrO_2/GCE for varying sulfinpyrazone concentrations are illustrated in Fig. 11. Under optimized experimental conditions, the peak current exhibited a linear dependence on sulfinpyrazone concentration within the range of 0.025–100 μM. The corresponding calibration equation was established as I_p (μA) = 0.00578 C (μM) – 0.3874, with a correlation coefficient of R^2 = 0.999 (Fig. 12), indicating excellent linearity. The limit of detection (LOD) was calculated using the formula LOD = 3σ/m, where m represents the slope of the calibration curve and σ denotes the standard deviation of the blank signal. The LOD for sulfinpyrazone was determined to be 28 nM, demonstrating high sensitivity of the developed electrode. A comparison of the analytical performance of the Ag@ZrO_2/GCE with other recently reported modified electrodes for sulfinpyrazone determination is summarized in Table 1. The proposed Ag@ZrO_2/GCE exhibits a broader linear range and a lower detection limit than several previously reported sensors, confirming its superior electrochemical performance and suitability for sensitive sulfinpyrazone quantification.

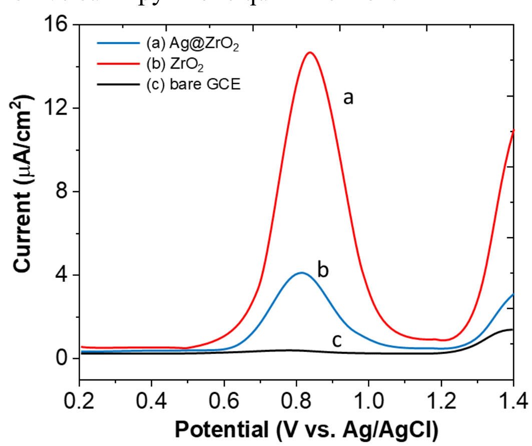

Fig. 9. Differential pulse voltammetric (DPV) responses of (c) bare GCE, (b) ZrO_2/GCE, and (a) Ag@ZrO_2/GCE electrodes recorded within a potential range of 0.2–1.4 V at a scan rate of 25 mV s^{-1} in 0.1 M phosphate buffer (pH 6.0) containing 5.0 μM sulfinpyrazone.

The differential pulse voltammetric response of a 5.0 μM sulfinpyrazone solution was recorded using six independently fabricated Ag@ZrO_2/GCE electrodes prepared under identical conditions. The relative standard deviation (RSD) for the peak current response was found to be 2.87%, indicating excellent reproducibility of electrode fabrication and measurement consistency. The potential interference effects of common inorganic ions and organic compounds (each at a concentration of 50 µM) on the voltammetric detection of 5.0 µM sulfinpyrazone were also investigated under optimized conditions. As illustrated in Fig. 13, the anodic peak current of sulfinpyrazone remained nearly unchanged in the presence of these interfering species, suggesting that the Ag@ZrO_2/GCE sensor exhibits high selectivity. This observation confirms that the proposed electrode can reliably detect sulfinpyrazone even in complex clinical matrices containing coexisting substances.

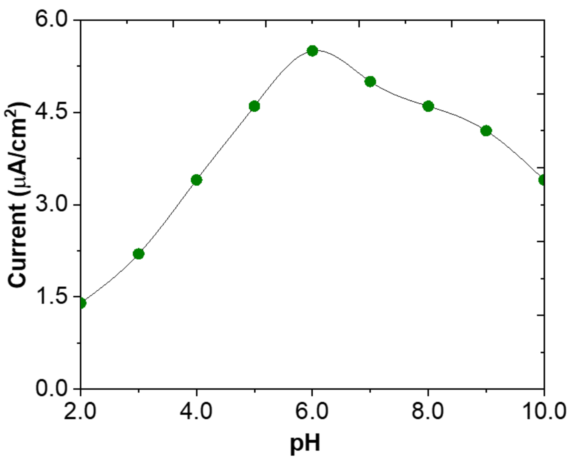

Fig. 10. Variation of peak current with pH for the Ag@ZrO_2/GCE electrode in 0.1 M phosphate buffer containing 6.0 µM sulfinpyrazone.

The practical applicability of the fabricated Ag@ZrO_2/GCE sensor was evaluated through recovery studies using spiked human serum samples. Serum aliquots collected from healthy volunteers were stored at 4 °C, centrifuged at 3000 rpm for 15 min, and filtered to remove proteins and other impurities. To minimize matrix interference, 1.0 mL of the supernatant was diluted tenfold with 0.1 M phosphate buffer (pH 6.0) before direct voltammetric analysis, without further preprocessing. As summarized in Table 2, the recovery values exceeded 96%, with a relative standard deviation (RSD) below 0.22%, confirming excellent accuracy and precision. These results demonstrate that the Ag@ZrO_2/GCE sensor is highly suitable for accurate electrochemical determination of sulfinpyrazone in real biological samples.

Additionally, to evaluate the long-term stability and reproducibility of the Ag@ZrO_2/GCE, DPV measurements were conducted for a 5.0 µM sulfinpyrazone solution over five consecutive days. The test was performed using five independently prepared modified electrodes, each subjected to four repeated measurements per day. The oxidation peak current (I_p) of sulfinpyrazone exhibited minimal variation, retaining 99.69%, 99.20%, 98.90%, and 98.40% of its initial response over successive trials. These findings confirm the Ag@ZrO_2/GCE sensor's excellent reproducibility, operational stability, and long-term reliability for electrochemical detection of sulfinpyrazone. The synergistic connection between ZrO_2 and Ag ensures the stability of our sensor. This interaction not only improves the sensor's performance but also gives it dependable long-term sensing capabilities without noticeable performance loss or deterioration. This proposed method not only improves the electrochemical response, stability, and sensitivity for sulfinpyrazone detection, but it also establishes a new standard for the creation of electrochemical sensors that are more dependable and efficient.

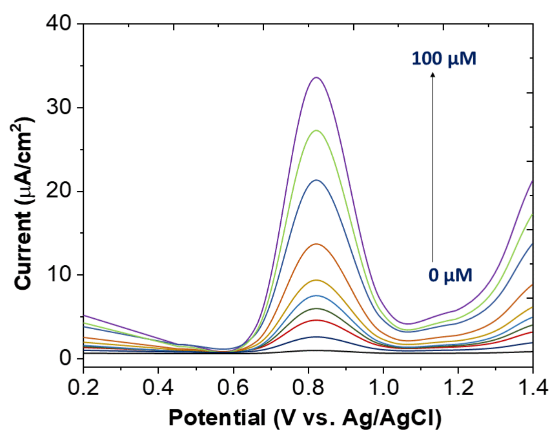

Fig. 11. Differential pulse voltammetric responses of the Ag@ZrO_2/GCE electrode obtained for successive additions of sulfinpyrazone (0.025 µM to 100 µM) in 0.1 M phosphate buffer (pH 8.0) at a scan rate of 25 mV s^{-1}.

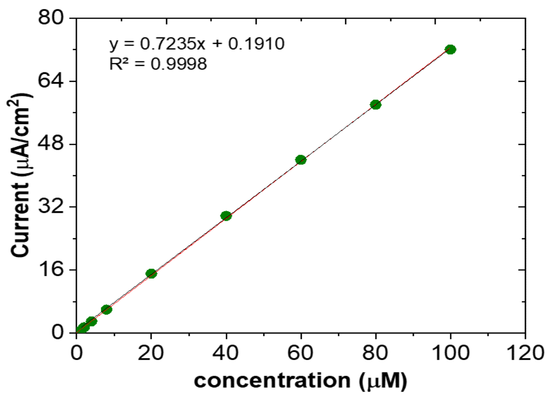

Fig. 12. Calibration plot illustrating the differential pulse voltammetric (DPV) response of the Ag@ZrO_2/GCE electrode to successive additions of sulfinpyrazone in 0.1 M phosphate buffer (pH 8.0) at a scan rate of 25 mV s^{-1}.

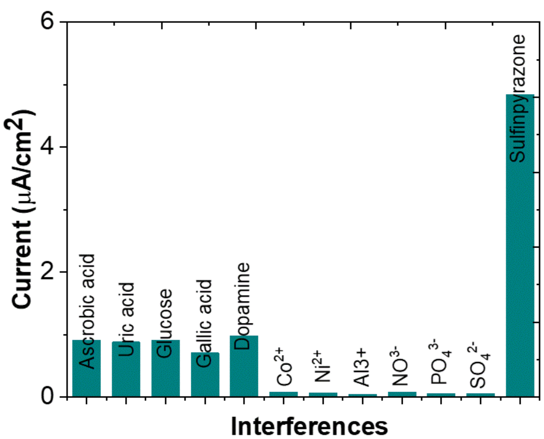

Fig. 13. Differential pulse voltammetric (DPV) responses recorded at the Ag@ZrO_2/GCE electrode at an applied potential of 0.64 V in 0.1 M phosphate buffer (pH 8.0) during successive additions of 10 μM sulfinpyrazone and 50 μM interfering species.

Antibacterial efficacy

The antibacterial efficacy of green-synthesized ZrO_2 and Ag@ZrO_2 nanoparticles, *Sargassum polycystum* extract, and the standard antibiotic gentamycin was evaluated against two bacterial strains *Bacillus subtilis* (Gram-positive) and *Escherichia coli* (Gram-negative). The synthesized ZrO_2 and Ag@ZrO_2 nanoparticles exhibited notable inhibition zones of 6.8, 7.2, and 6.4 mm against *B. subtilis*, and 3.2, 4.4, and 5.6 mm against *E. coli*, respectively. Both the *Sargassum polycystum* extract and its derived nanocomposites demonstrated stronger antibacterial activity compared to the conventional antibiotic gentamycin as shown in Table 3. The antimicrobial action of ZrO_2 and Ag@ZrO_2 nanoparticles stems from their capacity to attach to bacterial cell membranes, infiltrate them, and gather within the lipid bilayer. This interaction disrupts vital cellular processes like enzyme activity, DNA replication, and ATP production, which eventually results in the breakdown and death of the bacterial cell [28].

Table 1. Comparative summary of the present work with previously reported electrochemical sensors for drug monitoring available in the literature.

Technique	Electrode	Analytical linear range (nM)	LOD (nM)	Ref.
CV	Serum albumin-Ag nanoprobe/polypyrrol imprinted	0.5-200	400	34
DPV	Boron-doped diamond electrode	1.9–247	57	35
DPV	Au Nanoparticles/Graphen/GCE	1.0×10^3 - 2.0×10^6	5000	36
DPV	Hemoglobin/didodecyldimethylammonium bromide /SWNTs/Au electrode	1.4×10^3 - 1.0×10^5	2800	37
DPV	Nano-TiO_2/Nafion composite film/GCE	500-200	1.0×10^6	38
DPV	CD-GNs/GCE	1000-200	1.0×10^5	39
DPV	Ag@ZrO_2/GCE	0.05-100	28	Presnet work

Table 2. The results obtained from differential pulse voltammetry measurements using Ag@ZrO_2/GCE in a 0.1 M phosphate buffer solution prepared with a real urine sample for sulfinpyrazone determination (n = 4).

Samples	Spiked (μM)	Detected (μM)	Recovery (%)	RSD (%)
Serum	2	1.92	98.40	0.22
	5	4.80	98.00	0.10
	10	9.50	96.80	0.18
	20	19.50	99.00	0.11

Table 3. Antibacterial activity of ZrO_2 and Ag@ZrO_2 nanoparticles

Bacterial	Zone of inhibition (mm)

strains	Gm	ZrO_2			Gm	$Ag@ZrO_2$		
	25 µL	25 µL	50 µL	100 µL	25 µL	25 µL	50 µL	100 µL
B. Subtilis	6.5	6.8	7.2	6.4	6.8	6.6	7.2	8.2
E. Coli	5.2	3.2	4.4	5.6	7.2	3.5	4.2	4.8

IV. CONCLUSION

This study demonstrates a simple, cost-effective, and environmentally sustainable approach for synthesizing ZrO_2 and $Ag@ZrO_2$ nanocomposites using an aqueous extract of *Sargassum polycystum* seaweed as a natural reducing and stabilizing agent. The fabricated $Ag@ZrO_2$-modified glassy carbon electrode ($Ag@ZrO_2$/GCE) exhibited markedly superior electrochemical performance for sulfinpyrazone detection compared to both the bare GCE and ZrO_2/GCE, consistent with findings reported in related literature. The enhanced sensing behavior can be attributed to the synergistic interaction between silver and zirconia, which collectively enhanced the sensor's stability, sensitivity, and selectivity. The developed method achieved a broader linear response range and a lower detection limit than previously reported electrochemical sensors, underscoring its high analytical efficiency and potential for sustainable monitoring of anticancer drugs. In addition to its electrochemical advantages, the green-synthesized $Ag@ZrO_2$ nanocomposites demonstrated notable antibacterial activity against selected Gram-negative bacterial strains, indicating their promise for biomedical and clinical applications. Overall, the findings establish a robust foundation for developing efficient, low-cost, and eco-friendly electrochemical sensing platforms for pharmaceutical and biological analyses. The proposed $Ag@ZrO_2$/GCE sensor exhibited excellent sensitivity, reproducibility, and stability in the detection of sulfinpyrazone from serum samples, highlighting its applicability in real-world clinical diagnostics.

V. CONFLICT OF INTEREST

All authors declare that they have no conflicts of interest concerning this work.

REFERENCES

[1] Aigbe U.O., Osibote O. A., Green synthesis of metal oxide nanoparticles, and their various applications, Journal of Hazardous Materials Advances, 13, 2024, 100401, https://doi.org/10.1016/j.hazadv.2024.100401.

[2] Meena J., Sivasubramaniam S., David E., Santhakumar K., Green supercapacitors: review and perspectives on sustainable template-free synthesis of metal and metal oxide nanoparticles, RSC Sustainability, 2, 5, 2024, 1224-1245, https://doi.org/10.1039/d4su00009a.

[3] Kousar R., Zia Ul H.K., Sana S., Jingyu S., Nawshad M., Noor S.S., Jibran I., Syed K., Mohamed A.S., Synergetic comparative study: Photocatalytic and biological investigations of green-synthesized metal oxide nanoparticles, Nano-Structures & Nano-Objects, 38, 2024,101184, https://doi.org/10.1016/j.nanoso.2024.101184.

[4] Hussein T., Ali B., Tuqa A., Nirmalendu B., Azher M. A., Jameel M.D., Hayder I.M., Bhupendra K.S., Dipankar P., Praveen B. Current developments in the use of nanotechnology to enhance the generation of sustainable bioenergy, Sustainable Materials and Technologies, 43, 2025, e01266, https://doi.org/10.1016/j.susmat.2025.e01266.

[5] Mansour S.A.G., Mohyeddine A., Samir O.M., Abdulqawi N., Ayman A. R.S., Ebkar Abdo A.S., Effect of single and combined (core/shell) biosynthesis of nanoparticles (Ag and ZnO) on their photocatalytic and antimicrobial activities, Kuwait Journal of Science, 52, 2, 2025, 100356, https://doi.org/10.1016/j.kjs.2024.100356.

[6] Houda E., Victor O. M., Gloria A., Matthew M., Tasneema I., Ashiwin V., Navid R. M., Microalgae as sustainable bio-factories for nanoparticle biosynthesis: Progress and challenges, Bioresource Technology Reports, 2025, 102089, https://doi.org/10.1016/j.biteb.2025.102089.

[7] Bartholomew S.A., Olumayowa M.O., Modupe S.A., Oluwaseun A.F., Oluwadara P.O., Ayomide E.F., Damian C.O., Olubukola O.B., Biosynthesis of nanoparticles using microorganisms: A focus on endophytic fungi, Heliyon, 10, 21, 2024, e39636, https://doi.org/10.1016/j.heliyon.2024.e39636.

[8] P. Barciela, M. Carpena, Ning-Yang Li, Chao Liu, S.M. Jafari, J. Simal-Gandara, M.A. Prieto, Macroalgae as biofactories of metal nanoparticles; biosynthesis and food applications, Advances in Colloid and Interface Science, 311, 2023, 102829, https://doi.org/10.1016/j.cis.2022.102829.

[9] Aman K. Chitoria, Arshid Mir, M.A. Shah, A review of ZrO_2 nanoparticles applications and recent advancements, Ceramics International, 49, 20, 2023, 32343-32358, https://doi.org/10.1016/j.ceramint.2023.06.296.

[10] Anuj M., Gourav K., Bhavna S., Tim P., Vinod K., Suresh K., Naveen K., ZrO_2 based nanostructures: A sustainable, economical, green and efficient organocatalyst, Journal of Molecular Liquids, 398, 2024, 124223, https://doi.org/10.1016/j.molliq.2024.124223.

[11] L. Keerthana, C. Sakthivel, I. Prabha, MgO-ZrO_2 mixed nanocomposites: fabrication methods and applications, Materials Today Sustainability, 3–4, 2019, 100007, https://doi.org/10.1016/j.mtsust.2019.100007.

[12] Elizabeth K., Bharat G., Zefeng Y., Tamas V., Kenneth G., Arun D., David S., Investigating zirconium alloy corrosion with advanced experimental techniques: A review, Journal of Nuclear Materials, 585, 2023, 154586, https://doi.org/10.1016/j.jnucmat.2023.154586.

[13] Nayem H., Md Hosne M., Amran H., Fardin K., Juhi Jannat M., Mohammad Asaduzzaman Chowdhury, Advances of plant and biomass extracted zirconium nanoparticles in dental implant application, Heliyon, 9, 5, 2023, e15973, https://doi.org/10.1016/j.heliyon.2023.e15973.

[14] Ehsan R., Saeid B., Fatemeh K., A comparative study on antibacterial properties of EuO, CuO, and ZnO dopped ZrO2 sol-gel coatings, Ceramics International, 50, 24, 2024,52205-52212, https://doi.org/10.1016/j.ceramint.2024.07.364.

[15] Sarita A., Monika N., Neeraj D., Sandeep K., Synthesis of ZrO_2 and its composite with activated carbon for lead adsorption and antibacterial applications, Hybrid Advances, 7, 2024, 100321, https://doi.org/10.1016/j.hybadv.2024.100321.

[16] Tadanobu I., Mary E.B., Eva J. Chow, Determinantion of sulfinpyrazone in serum by high-performance liquid chromatography, Journal of Chromatography A, 104, 1, 1975, 165-169, https://doi.org/10.1016/S0021-9673(01)85501-1.

[17] Garanin, Y., Shakirzyanov, R., Borgekov, D. et al. Study of morphology, phase composition, optical properties, and thermal stability of hydrothermal zirconium dioxide synthesized at low temperatures. Sci Rep 14, 29398 (2024). https://doi.org/10.1038/s41598-024-80399-x

[18] Amol N., Trupti P., Suresh G., Khanderao P., Shreyas P., A Review on Plant Extract Mediated Green Synthesis of Zirconia Nanoparticles and Their Miscellaneous Applications, Journal of Chemical Reviews (J. Chem. Rev.), 2019, 1(3), 154-163.

[19] P. Jakobsen, A.Kirstein Pedersen, Determination of sulfinpyrazone and two of its metabolites in human plasma and urine by gas chromatography and selective detection, Journal of Chromatography B: Biomedical Sciences and Applications, 163, 3, 1979, 259-269, https://doi.org/10.1016/S0378-4347(00)81413-9.

[20] Thorir D.B., Katherine M.W., Philip A.R., David G.S., High-performance liquid chromatographic analysis of sulfinpyrazone and its metabolites in biological fluids, Journal of Chromatography B: Biomedical Sciences and Applications, 181, 3–4, 1980, 417-425, https://doi.org/10.1016/S0378-4347(00)81144-5.

[21] J.G. Suma, Yuvarajgouda N. Patil, Manjunath B. Megalamani, S.K. Rajappa, Sharanappa T. Nandibewoor, Sensitive electrochemical analysis of uricosuric drug sulfinpyrazone using a graphene-based sensor: A first voltammetric approach, Next Materials, 7, 2025,100346, https://doi.org/10.1016/j.nxmate.2024.100346.

[22] Sandeep R.K., Yuvarajgouda N.P., Manjunath B.M., Sharanappa T.N., Enhancing Sulfinpyrazone Determination via Electrochemistry: Development of a S-Doped CoFe2O4 Modified Sensor, Journal of The Electrochemical Society, 172, 1, 017518, DOI 10.1149/1945-7111/adaa25

[23] Sumayya M. AnsariBhavesh B. SinhaDeodatta PhaseDebasis SenPulya U. SastryYesh D. Kolekar Chintalapalle V. Ramana, Particle Size, Morphology, and Chemical Composition Controlled CoFe2O4 Nanoparticles with Tunable Magnetic Properties via Oleic Acid Based Solvothermal Synthesis for Application in Electronic Devices, ACS Appl. Nano Mater. 2019, 2, 4, 1828–1843, https://doi.org/10.1021/acsanm.8b02009.

[24] Reddy P.P., Sandhya P., Ayyappa B., Nagendra K.P.V., Suvardhan K., Electrochemical non-enzymatic strategy with green synthesized Fe_2O_3-CuO nanocomposite for detection of amiprofos-methyl herbicide in industrial effluents and soils, Chemical Physics Impact, 6,2023, 100195, https://doi.org/10.1016/j.chphi.2023.100195.

[25] Ali R.J., Mohammad M.K. A comprehensive review on roles of electrochemical approaches in drug delivery, Sensing and Bio-Sensing Research, 47, 2025, 100742, https://doi.org/10.1016/j.sbsr.2025.100742.

[26] Ayesha Q., Afzal S., Faiza J.I., Abdul H., Abid Zia M., Electrochemical analysis of anticancer and antibiotic drugs in water and biological specimens, RSC Advances,14, 49, 2024, 36633-36655, https://doi.org/10.1039/d4ra05685j.

[27] Supriya G., Reddy P.P., Sandhya P., Venkata N.K.P., Biosynthesis of Pd@$CuCo_2O_4$ nanocomposites for sensitive electrochemical detection of doxorubicin and their biological activities, International Journal of Electrochemical Science, 20, 11, 2025, 101185, https://doi.org/10.1016/j.ijoes.2025.101185.

[28] Tuan D. D., Nhu-Nang V., Thi Linh G.H., Phuong N., Metal-organic framework (MOF)-based materials for photocatalytic antibacterial applications, Coordination Chemistry Reviews, 523, 2, 2025, 216298, https://doi.org/10.1016/j.ccr.2024.216298.

[29] S. Gumma, R.P. Puthalapattu, S. Punyasamudram, P.R. Kanuparthy, P. V. Nagendra Kumar. Eco-Friendly Phytochemical-Derived Co3O4@Ag Nanoparticles for Ethanol Oxidation and Antibacterial Activity. Asian Journal of Green Chemistry, 8(5) 2024, 560-578.https://doi.org/10.48309/ajgc.2024.456977. 1504.

[30] H.C. Sathisha, Anitha, G. Krishnamurthy, G. Nagaraju, Facile green synthesis of ZnO/ZrO_2 nanocomposite for photocatalytic degradation and chromium (VI) reduction, Journal of Crystal Growth, 651, 2025, 128009, https://doi.org/10.1016/j.jcrysgro.2024.128009.

[31] Mehdi M., Mahmoud N., Sajadi S.M., Facile synthesis of Ag/ZrO_2 nanocomposite as a recyclable catalyst for the treatment of environmental pollutants, Composites Part B: Engineering, 185, 2020, 107783, https://doi.org/10.1016/j.compositesb.2020.107783.

[32] Ling Z., Jie Y., Xinyue W., Gao S., Fan L., Lijun Y., Jumei L., Ag nanoparticles decorated Ag@ZrO_2 composite nanospheres as highly active SERS substrates for quantitative detection of hexavalent chromium in waste water, Journal of Molecular Liquids, 319, 2020, 114158, https://doi.org/10.1016/j.molliq.2020.114158.

[33] Shuhua L., Yuting H., Yiwen Z., Li L. Open three-dimensionally ordered macroporous composite Ag/TiO2: synthesis and multi-modes photocatalytic degradation Malachite green, Desalination and Water Treatment, 233, 2021, 399-407, https://doi.org/10.5004/dwt.2021.27548.

[34] S.I. Khan, A. Hassan, R. Bano, M.A. Gilani, J.L. Marty, H. Zhang, A. Hayat, An innovative and universal dual-signal ratiometric spectro-electrochemical imprinted sensor design for sandwich type detection of anticancer-drug, gemcitabine, in serum samples; cross validation via computational modeling, Talanta 267 (2024) 125233.

[35] I. Rus, A. Pusta, M. Tertiș, C. Barbalat, I. Tomuța, R. Sandulescu, C. Cristea, Gemcitabine direct electrochemical detection from pharmaceutical formulations using a boron-doped diamond electrode, Pharmaceuticals 14 (2021) 912.

[36] Y. Du, M. Dou, W. Ma, X. Wang, Z. Gu, X. Deng, Preparation of graphene-copper nanocomposite for constructing electrochemical sensor for Paclitaxel anti-cancer drug detection in Taxus Chinensis, Int. J. Electrochem. Sci. 12 (2017) 2563–2572.

[37] Y. Zhang, W. Cheng, S. Li, N. Li, Direct electron transfer of hemoglobin on DDAB/SWNTs film modified Au electrode and its interaction with Taxol, Colloids Surf. A Physicochem. Eng. Asp. 286 (2006) 33–38.
[38] B. Rezaei, N. Askarpour, A.A. Ensafi, A novel sensitive doxorubicin impedimetric immunosensor based on a specific monoclonal antibody-gold nano particle-sol-gel modified electrode, Talanta 119 (2014) 164–169.
[39] J.G. Guan, Y.Q. Miao, Q.J. Zhang, Impedimetric biosensors, J. Biosci. Bioeng. 97 (2004) 219–226.